Scanning-tunneling-microscopy study of tip-induced transitions of dislocation-network structures on the surface of highly oriented pyrolytic graphite

S. R. Snyder, W. W. Gerberich, and H. S. White
Department of Chemical Engineering and Materials Science, University of Minnesota, Minneapolis, Minnesota 55455
(Received 28 August 1992)

Scanning-tunneling-microscopy observations of a reversible, tip-induced transition between triangular- and star-shaped networks of partial dislocations on the basal (0001) plane of highly oriented pyrolytic graphite are reported. The transition between network geometries results from small variations (0.14 V) in the tip-to-substrate voltage bias and is attributed to shear-induced motion of partial dislocations. The shear stress required for the transition is estimated to be 5 MPa. Dislocation motion occurs over distances of tens of nanometers on the time scale of several minutes, allowing the dynamics of the transition between the two networks to be observed in real time. Atomically resolved images near a dislocation show distortions of the atomic lattice that are consistent with glide of the surface basal plane. Analysis of the separation distance between pairs of dislocations yields a surface stacking-fault energy of 2.1–4.5 mJ/m^2.

I. INTRODUCTION

Highly oriented pyrolytic graphite (HOPG) has been used extensively as a substrate in scanning-tunneling-microscopy (STM) investigations[1–3] because it is readily cleaved to yield atomically flat stable surfaces. Although Lipson and Stokes[4] reported in 1942 that natural-graphite samples are comprised of 5–15 % rhombohedral graphite, intermixed with the more abundant hexagonal graphite, STM observations of the rhombohedral structure have only been reported once.[5] The percentage of rhombohedral graphite in synthetic HOPG, which is commonly used in STM investigations, depends on the annealing and quenching procedures used in the specimen preparations, and is typically on the order of a few percentile.[4,6,7]

Rhombohedral graphite differs from hexagonal graphite in the stacking of atomic planes parallel to the *c* axis. Rhombohedral graphite has an *abcabc* stacking sequence while hexagonal graphite has an *abab* stacking sequence [Fig. 1(a)]. Previous transmission electron microscopy (TEM) and x-ray-diffraction studies have demonstrated that the rhombohedral phase is contained within stacking faults in pyrolytic graphite. The stacking faults are generally observed in TEM as networks of partial dislocations that separate regions of faulted (rhombohedral) and unfaulted (hexagonal) graphite. By displacement of one or more atomic plane(s) normal to the *c* axis, the transition between the rhombohedral and hexagonal phases within the network may be represented as

$$ababa\ldots\leftrightarrow abcab\ldots. \quad (1)$$

The resulting "glide" of an atomic plane, shown in Fig. 1(b), defines the partial dislocations in graphite and has been detailed by Delavignette and Amelinckx,[8] Williamson,[9] and Lipson and Stokes.[4] An in-plane transition between the two phases (which are bounded by the partial dislocation), requires distortion of the atomic arrangement and/or cleavage of carbon-carbon bonds. However, breakage of in-plane carbon-carbon bonds is unlikely based on energetic considerations. Low-energy, in-plane distortions of carbon-carbon bonds are likely to occur along the dislocation for small distances of in-plane glide (approximately one atomic row), although they are probably less severe than suggested in Fig. 1(b). The in-plane atomic bond distances (1.42 Å) and interlayer separation (3.35 Å) of the pure hexagonal and rhombohedral phases removed from the dislocation are identical.

In this paper, STM images of large-scale triangular- and star-shaped dislocation networks that separate regions of hexagonal and rhombohedral graphite on the basal surface of a HOPG sample are reported. A reversi-

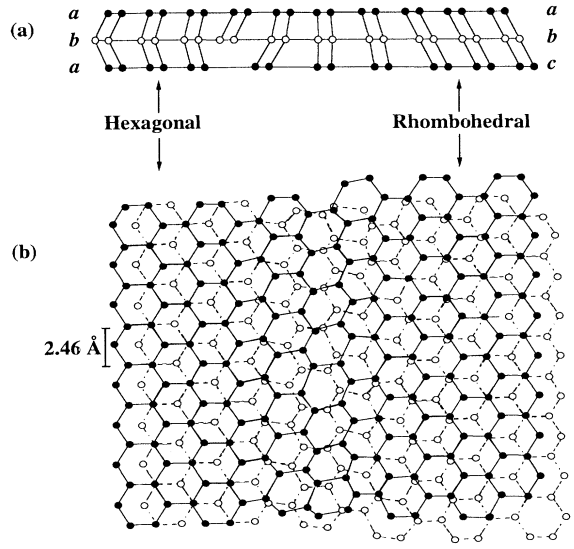

FIG. 1. (a) Schematic diagram showing a basal dislocation in graphite between hexagonal and rhombohedral graphite. (b) Projection of a 60° basal plane dislocation on the *c* plane. Two planes are shown: the solid and dashed hexagons are in adjacent planes.

ble transition between the triangular- and star-shaped networks is observed that is a function of the bias voltage between the STM tip and HOPG substrate. The transition results in the interconversion of hexagonal and rhombohedral graphite, indicating the reversibility of Eq. (1). Atomically resolved images of the transition region yield direct structural details of the atomic arrangement along the partial dislocation. The energy between the surface dislocations in the network is also determined and compared to bulk values obtained from previous TEM studies.

II. EXPERIMENT

Tunneling experiments were performed using a commercial STM (Nanoscope II, Digital Instruments Inc., Goleta, CA). Images were recorded in the constant current mode using a mechanically cut Pt-Rh (80–20 %) tip. Tunneling currents, bias voltages (reported as sample versus tip), and scan rates are reported in each figure caption. All images, except for those in Fig. 3, have been low-pass filtered once. Images in Fig. 3 have one fast Fourier transform applied to them. Experiments were performed in air on a freshly cleaved sample of HOPG (Union Carbide grade B).

III. RESULTS AND DISCUSSION

Our results are presented in the following order. In Sec. III A, we describe the general features of the dislocation network investigated in this study. In Sec. III B, atomically resolved images of the faulted structure are presented which provide details of the distortion of carbon-carbon bonds along a dislocation. The microscopically and atomically resolved images presented in these sections are consistent with the structure shown in Fig. 1 and with the notion that the faulted region results from in-plane glide of the basal plane. In Sec. III C, images of reversible STM tip-induced transitions between triangular- and star-shaped networks are presented and analyzed in terms of the extension and contraction of dislocation nodes. A preliminary analysis of the tip-induced transition dynamics is also presented, including calculations of an average dislocation velocity from a time-resolved series of images. In Sec. III D, we calculate the energy of the dislocation array from STM images and estimate the tip-induced shear forces required to cause the transition between network geometries. We show that the required shear forces are of the same order of magnitude as tip-substrate forces required to image HOPG samples.

A. Dislocation network

Figure 2(a) shows a STM image of a triangular-shaped network of partial dislocations on the HOPG surface. On average, the bases and heights of the triangles were 75 and 110 nm, respectively. Triangular arrays similar to that shown in Fig. 2 have been previously observed in STM (Ref. 5) and TEM (Refs. 8 and 9) investigations. The triangular network encompassed a total area estimated to be in excess of 4 μm^2.

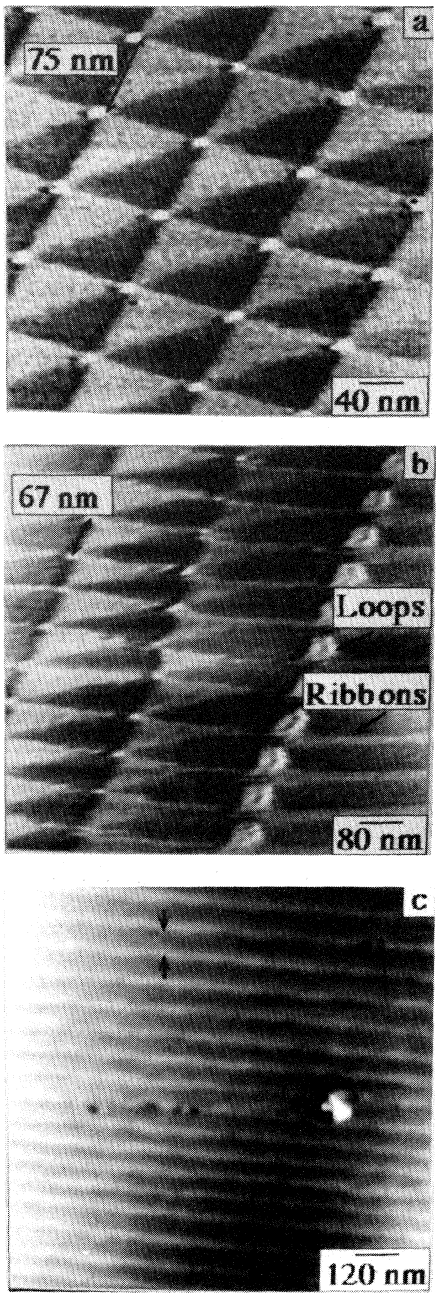

FIG. 2. STM image of (a) a 400 nm×400 nm area of a triangular array on the (0001) plane of HOPG. The array consists of alternating faulted (rhombohedral graphite, light triangular regions) and unfaulted (hexagonal, dark triangles). Sample bias voltage, tunneling current, and scan rate were 0.24 V, 0.37 nA, and 26 Hz, respectively. (b) 800 nm×800 nm area to the right of the array in (a) showing a row of prismatic dislocation loops which form the boundary between the triangular array and rows of ribbons. Sample bias voltage, tunneling current, and scan rate were 0.12 V, 0.6 nA, and 26 Hz, respectively. (c) 1200 nm×1200 nm area to the right of the triangular array showing a large area covered by rows of ribbons. The ribbons terminate at a defect site on the graphite. Sample bias voltage, tunneling current, and scan rate were 0.10 V, 0.78 nA, and 26 Hz, respectively.

One edge of the network was examined in detail. Along this edge, a row of elliptical dislocation loops defined the boundary between one corner of each triangle and a long straight ribbon, Fig. 2(b). The dislocation loops are ~50 nm wide and ~47 nm long, and have an apparent displacement of 3.9 Å above the surrounding surface. The central depression defined by the loop is ~2.9 Å deep. Elliptical and quasihexagonal dislocation loops have been previously identified on the graphite basal plane by Delavignette and Amelinckx[8] and are believed to pin dislocations associated with in-plane glide, consistent with the termination of the triangular network. The ribbons emerging from the triangular array are comprised of two partial dislocations *(vide infra)* separated by 12–25 nm; the center-to-center distance between ribbons is equal to the base width of a triangle within the network (75 nm). The partial dislocations form a large network of parallel ribbons [at least 2.5×2.5 μm, Fig. 2(c)] and appear to terminate at a poorly resolved defect (not shown) which is probably associated with plastic deformation during cleavage of the sample. This conclusion is supported by previous TEM observations that suggest that the number density of stacking-fault arrays in pyrolytic graphite significantly increases with mechanical crushing of the sample and that dislocations end at the edge of a flake, cleavage step, or low angle boundary.[9]

Williamson[9] attributed the diffraction contrast in TEM images of triangular-shaped arrays, which are nearly identical to the array in our STM images (Fig. 2), to rhombohedral stacking faults enclosed between partial dislocations in the hexagonal structure. The glide of atomic planes observed in HOPG by TEM is generally in the form of arrays of partial dislocations which can combine into a perfect basal screw dislocation following the general reaction

$$1/3a\,[1\bar{1}00]+1/3a\,[10\bar{1}0]=1/3a\,[2\bar{1}\bar{1}0]\ . \qquad (2)$$

The partials describe the translocation needed to convert a *b* layer to a *c* layer, Eq. (1), and form the boundary between the hexagonal (unfaulted) and the rhombohedral (faulted) phases. Based on the structural assignments from previous TEM and electron-diffraction analyses,[8,9] and the geometrical similarity of the network array in both STM and TEM images, we have previously assigned the lighter triangles in the STM images to the rhombohedral crystal structure and the darker triangles to the hexagonal crystal structure.[5] Similarly, the rhombohedral and hexagonal structures are assigned to the bright and dark regions, respectively, of the ribbons extending from the triangular-network edge.

The observed contrast in the image of the triangular-shaped network is dependent on the STM sample bias voltage and tunneling current. In the image shown in Fig. 2(a), which was recorded at a bias voltage V_t (substrate vs tip), of 0.24 V and set-point current I_t of 0.37 nA, the lighter contrast triangles correspond to an apparent displacement of 1.7 Å above the darker triangles. The intersection of three triangles is defined by a brighter circular region (diameter ~20 nm) which is displaced 4.3 Å above the dark triangular regions. When the STM settings were changed to $V_t=0.53$ V and $I_t=2.4$ nA, the contrast between the light and dark triangles disappears and the intersection points appeared displaced by 1.2 Å above the surface. At $V_t=-0.22$ V and $I_t=0.37$ nA, the contrast difference between the dark and light triangles reduced to 0.8 Å and the intersection points disappeared. We note that the interplanar spacings of hexagonal and rhombohedral graphite are identical, and that the triangular-network structure is consistent with the assumption that glide is contained within the basal plane. Thus the observed contrast cannot result from an actual topographical *z* displacement between the faulted and unfaulted regions. A similar contrast dependence on V_t and I_t was also noted in previous work[5] and discussed in terms of the differences in electronic and elastic properties of hexagonal and rhombohedral graphite. However, no unambiguous explanation of the observed contrast has yet been forwarded.

A recent publication by Garbarz *et al.*[10] has associated a superlattice hexagonal network (~35-Å periodicity) with an array of basal dislocations. Similar large-scale hexagonal structures with various periodicities have been observed in our laboratory and by others[11] and identified as a local misorientation of the top basal plane giving rise to a simple moiré pattern. However, we have never observed these structures near a large-scale dislocation network, such as that shown in Fig. 2.

The STM observations that we describe in detail below are based solely on continuous studies of the single dislocation network shown in Fig. 2 over a period of two days. While we have previously reported STM images of similar structures,[5] well-defined network arrays of this magnitude are infrequently encountered during STM imaging. Experimental measurements on the dislocation terminated with a tip crash which resulted in a marked decrease in image resolution. We were unable to relocate the network array using new atomically sharp tips.

B. Atomically resolved structure of a partial dislocation

Figure 3(a) shows an atomically resolved image near the center of a dark (unfaulted), triangular region. The atomic arrangement and spacing is consistent with the reported hexagonal structure of graphite, i.e., the periodicities[12] at 2.6 Å and the corresponding fast Fourier transform (FFT) of the image (inset) shows six equally spaced points with hexagonal symmetry. However, the atomic corrugation is 0.8 Å, larger than expected. Large corrugation amplitudes have previously been observed on hexagonal graphite and have been attributed to elastic interactions of the tip with the sample surface.[13,14] In regions far removed from the dislocation network, atomically resolved images of the graphite surface show a hexagonal symmetry with periodicities of 2.6 Å and a corrugation amplitude of 0.3 Å.

The observed periodicity and symmetry in the STM images are known to result from an inequivalence of the electron charge density between surface atoms on the basal plane of hexagonal graphite. The tunneling current density above surface atoms with neighboring atoms lo-

cated directly below in the second layer (and all subsequent layers) i.e., α sites, is significantly lower than for surface atoms which do not have neighboring atoms in the second layer, i.e., β sites [Fig. 1(a)]. Thus the bright spots observed in the STM images of hexagonal graphite correspond to regions of high current density above β-site atoms.

In bulk rhombohedral graphite, the inequivalence between in-plane neighboring atoms vanishes since all atoms in the bulk have one nearest-neighbor atom located directly in an adjacent plane. However, the calculations of Tomanék and Louie[15] suggest that the asymmetry in the charge density between neighboring in-plane atoms persists at the surface of rhombohedral graphite due to a surface state near the Fermi level that is localized on surface atoms which do not have neighboring atoms in the second layer [Fig. 1(a)]. Thus a similar corrugation and sixfold symmetry, as shown in Fig. 3(a) for hexagonal graphite, would also be expected for rhombohedral graphite. Unfortunately, we were not able to obtain a clear, atomically resolved image of a region within one of the bright triangles to test this prediction. However, Fig. 3(b) shows an atomically resolved image of a boundary between a light and dark triangle. (The image has been filtered using a FFT to improve contrast of the atomic-scale corrugation; this filtering reduces the contrast defining the boundary between the bright and dark triangles of the network. The periodic atomic-scale structure observed in the image prior to FFT filtering was not significantly affected by this process.) The atomic arrangement in the upper region of the image (corresponding to the faulted rhombohedral structure) shows a distorted hexagonal arrangement with periodicities of 2.4 and 2.8 Å. The atomic corrugation is 0.5 Å near the dislocation line drawn in the figure and decays to 0.3 Å away from the line in either direction. The FFT of the image (inset) shows four points in a rectangular arrangement, consistent with rectangular electron-diffraction patterns previously observed near dislocations on pyrolytic graphite.[16] A distortion in the hexagonal lattice can be seen by following the line drawn from the top left to the bottom right of the image at an angle of 62° to the direction of the dislocation (which is in the $\langle 1\bar{1}00 \rangle$ direction). The atomic rows along the $\langle 10\bar{1}0 \rangle$ direction shift a distance equivalent to one unit cell ($\sim$2.7 Å measured; 2.46 Å theory) in crossing the dislocation, consistent with the model structure shown in Fig. 1(b). The shift occurs over a distance of 12 hexagonal unit cells, which we interpret as defining the width of the dislocation. This finding is in agreement with previous estimates of the widths of partial dislocations in graphite ($\sim$20–30 unit cells[17]). Thermal and electronic drift in these measurements was negligible [see, for example, Fig. 3(a)], ruling out the possibility that the distortion of the hexagonal structure is a measurement artifact.

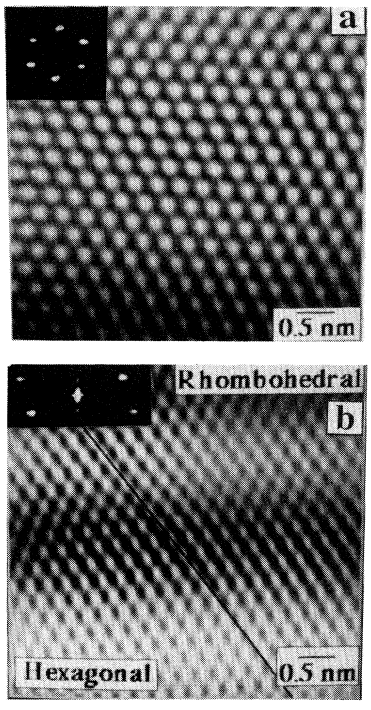

FIG. 3. (a) STM image of a 5 nm×5 nm area of a dark triangular region (unfaulted) showing the hexagonal arrangement of the graphite lattice. Bias voltage is 0.12 V and tunneling current is 0.7 nA. Inset: fast Fourier transform (FFT) of the image showing six bright spots characteristic of hexagonal graphite. Periodicities are 2.6 Å. (b) STM image of a 5 nm×5 nm area near the boundary between the lighter and darker triangular regions. The image shows glide of the basal plane by $\sim$1 unit cell. Bias voltage is 0.25 V and tunneling current is 1.7 nA. Inset: FFT of the image in (b) showing four bright spots in a rectangular pattern. Periodicities are 2.4 and 2.8 Å.

Close inspection of Fig. 3(b) shows that the hexagonal structure, albeit distorted, is maintained throughout the dislocation region. This finding, along with the observation that the contrast remains approximately uniform across this boundary, suggests that the charge-density asymmetry between neighboring surface atoms occurs *within the dislocation region,* as well as on the surface of the hexagonal (observed) and rhombohedral (predicted) phases. However, details of the atomic structure along the dislocation are not sufficiently well understood to analyze this finding in terms of electronic arguments.

C. Tip-induced dislocation motion and network transitions

A *reversible* transformation of the triangular-shaped network to a star-shaped network was observed while varying the bias voltage between 0.24 and 0.1 V, with the tunneling current maintained at 2.4 nA. Figure 4(a) shows a 500 nm×500 nm stable image of the dislocation network, shown previously in Fig. 1(a), several minutes after the bias had been decreased from 0.24 to 0.1 V. The network now appears to consist of alternating small and large triangles oriented at 180° from one another in the form of a distorted star. The sum of the lengths of the bases of small and large triangles (31 and 45 nm, respectively) is equivalent to the length of the base of an individual triangle (75 nm) in the network in Fig. 2(a). A similar equivalence exists between the heights of the triangles.

The sequence of images in Figs. 4(b)–4(d) demonstrates

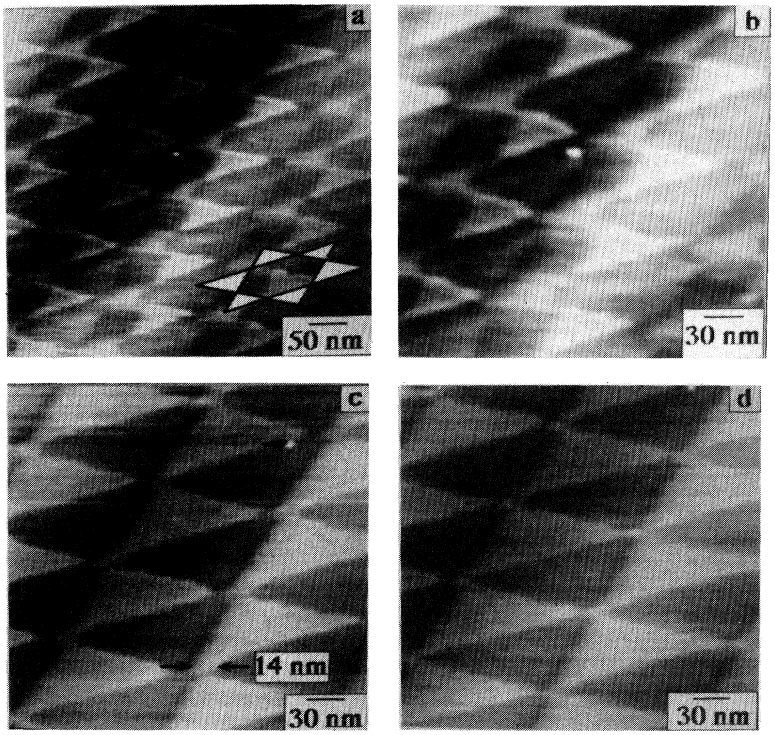

FIG. 4. STM images showing the voltage-induced transition of the star network to a triangular network as the bias voltage is changed from 0.10 to 0.24 V. [The white dot in the center of (a) can be used to identify the coordinates of the triangles in the sequence of images.] (a) 500×500 nm image of the star network obtained at 0.10 V. The star network is comprised of alternating small and large triangles pointing at 180° from one another. (b) 300 nm×300 nm image of the same area in (a). (c) 300 nm×300 nm image of the same area as in (b) showing the reappearance of the triangular network ~1 min after changing the bias voltage from 0.10 to 0.24 V. The triangles are no longer joined together at their vertices and the base of the triangles are trapezoidal shaped. (d) 300 nm×300 nm image of the same region taken 1 min later. The vertices of the triangles have intersected to form bright points. Tunneling currents are 2.4 nA and scan rates are 26 Hz.

the reversibility of the transition between the triangular- and star-shaped networks. Figure 4(b) is an enlargement of the image in Fig. 4(a) showing the star-shaped network at a bias voltage of 0.1 V. The image in Fig. 4(c) was recorded at ~1 min following a change in bias from 0.1 to 0.24 V. Each triangle is observed to have a lighter contrast trapezoidal-shaped band ~14 nm in width along its base (enlarged in Fig. 5). In fact, during the course of the transition from the star- to triangular-shaped network, the width of the band continuously decreased from a maximum value of ~30 nm. Bands from adjacent triangles overlap and the bright intersection points have not yet reappeared. The image in Fig. 4(d) was taken ~1 min after the image in Fig. 4(c) with the bias still at 0.24 V. The band at the base of the triangles has decreased to 9 nm, a few of the triangles have joined vertices forming the bright intersection points, and the heights and bases of the triangles have almost attained their original values. Continued scanning at a bias voltage of 0.24 V for several more minutes caused a complete return of the original triangular-shaped network shown in Fig. 2(a). This reversible transition between the triangular- and star-shaped network was reproducible during continuous imaging over a period of two days with no degradation of the network structures.

The mechanism for the transition between network geometries undoubtedly involves the movement of dislocations within the network. Figure 6(a) is a schematic of the triangular-shaped network showing an array of alternating shaded and unshaded triangles. The unshaded triangles (extended P nodes[18]) denote the rhombohedral (faulted) phase of graphite while the shaded triangles denote regions of hexagonal graphite. The boundaries enclosing the triangles are partial dislocations. At the intersection of the dislocations, corresponding to the bright spots in Fig. 2(a), the dislocations are contracted to form a K node. In the star-shaped network, Fig. 6(c), both the K and P nodes are fully extended and enclosed rhombohedral graphite.

The transition from the triangular-shaped network to the star-shaped network requires expansion of the contracted dislocations within the K nodes, as indicated in

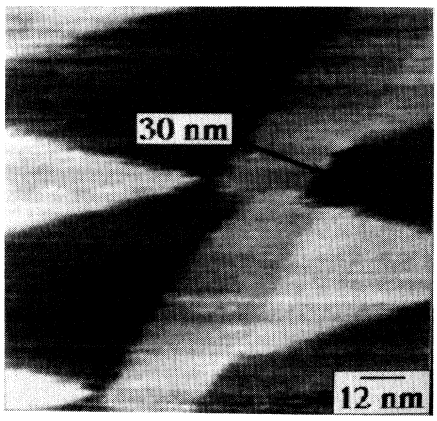

FIG. 5. A 125 nm ×125 nm STM image of the base region of a triangle showing the trapezoidal area of light contrast. Bias voltage is 0.24 V, tunneling current is 2.4 nA, and scan rate is 26 Hz.

Fig. 6. The transition can be viewed as resulting from the concerted motion of parallel dislocations along one of the three equivalent $\langle 10\bar{1}0 \rangle$ directions. Indeed, we were able to verify from STM images that motion of only one set of parallel partial dislocations occurred during the transition. Not coincidentally, motion occurred only for dislocations oriented nearly at right angles to the direction in which the tip was scanning (consistent with our analysis in Sec. III D that motion results from tip-induced shear stress). We note here, however, that although the shear forces due to scanning only act on a small fraction of the dislocation network at any one instant during imaging, the transition between the network geometries results from the concerted motion of numerous partials [for example, the concerted translation of three parallel partials is observed in the network transition shown in Figs. 4(b)–4(d)]. The translation of a set of parallel dislocations along only one of the three equivalent $\langle 10\bar{1}0 \rangle$ directions is shown schematically in Fig. 6(b).

The stability of the fully developed triangular- and star-shaped networks during prolonged STM scanning suggests that these structures represent metastable states. We believe that the structure shown in Fig. 6(b) depicts an unstable transition state captured in the image shown in Fig. 4(c) and enlarged in Fig. 5. The schematic structure of the intermediate shows that motion of only one parallel set of dislocations is consistent with the observation of a quasitrapezoidal region at the base of the triangle. As the partials move across the surface, the width of this trapezoidal region is expected to change, in agreement with the time-resolved images of the network transition.

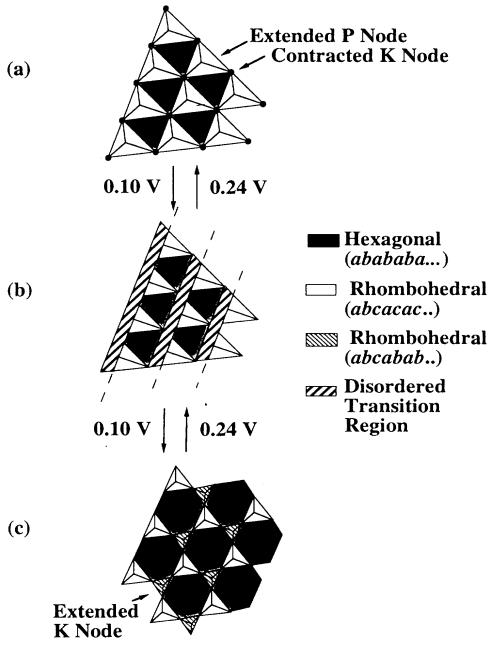

FIG. 6. Schematic showing the transition between the triangular- and star-shaped networks. (a) A triangular-network of extended P and contracted K modes. (b) Intermediate structure resulting from motion of one set of parallel partial dislocations (approximately left to right across the drawing). The intermediate structure has a trapezoidal band at the base of each bright triangle. (c) Star-shaped network of fully extended P and K nodes.

The extent to which the triangular-to-star transition occurs outside of the imaged area (following switching of the bias between 0.24 and 0.1 V) was not investigated. However, the ability to completely and rapidly cause the reverse transition suggests that the transition may be contained within a small local region. The reversibility of the transition also suggests that one of the two metastable states (triangles vs stars) results from a cancellation of shear forces and restoring forces that result from a local distortion of the network. We speculate that pinning of the dislocations at the network edge(s) by dislocation loops, such as those observed in Fig. 2(b) (as well as other surface features), might prevent motion of the dislocations near the network boundary. This would require the direction of the dislocation to deviate from the low-energy $\langle 10\bar{1}0 \rangle$ direction near the boundary, raising the energy of the network. When the shear force is reduced, as a result of changing the bias voltage (e.g., from 0.1 to 0.24 V), the energy stored in the network by distortion of the partials would necessarily be sufficient to drive the system back into the more stable state.

We were able to estimate average velocities of dislocation motion in the above experiments. From Figs. 4(b)–4(d), for example, the dislocation velocity can be approximated by the ratio of the distance that the triangles elongate to fuse at their vertices, relative to the time required for the complete transition between the triangular- and star-shaped networks ($\sim$2 min). From our observations, we estimate an average value of 10^{-10} m/sec, which is considerably smaller than values reported in the literature for a variety of materials (10^{-8}–10^{3} m/sec).[19] However, in macroscopic measurements of dislocation velocity, a shear stress is applied across the entire sample such that the resulting shear forces act (presumably uniformly) along the entire length of the dislocation. Obviously, in STM experiments, at any one instant, the tip-induced shear stress is highly localized over a short length of the dislocation. Thus it is not unexpected that the time-averaged dislocation motion resulting from a series of short-time pulses over the dislocation is correspondingly smaller. We did not investigate the distinct possibility that the dislocation velocity may depend on the scan rate as well as the applied bias.

D. Stacking-fault energy and shear stress for dislocation motion

Shear stresses resulting from interactions between the tip and graphite surface are responsible for dislocation motion. Graphite shear deformation, without cleavage of the basal plane, can only occur if there is a large compressive stress normal to the basal plane.[20] In addition, the rhombohedral phase is only produced when the hexagonal structure is under severe shear. Thus the triangle-to-star-shaped network transition requires that the tip-sample interaction is associated with both a nor-

mal compressive and shear stress. Evidence to support the presence of tip induced forces is evident in Figs. 2(b) and 4(a), where the dislocations at the bases of the triangles are bowed out normal to the direction of scanning.

If dislocation motion is due to shear stresses resulting from tip scanning, then changing the tip-to-sample distance should reveal this phenomenon. Indeed, the voltage-dependent transition between the triangular- and star-shaped networks can be interpreted in terms of the dependence of the tip-to-sample separation s on the voltage. Using the tunneling equation[21]

$$I \propto V \exp(-2\kappa_0 s) , \tag{3}$$

where I is the tunneling current, s is the tip-to-sample separation, V is the sample bias voltage, and $2\kappa_0$ (Å)$=1.025\sqrt{\phi_{\text{eff}}}$ [ϕ_{eff} (eV) is the effective barrier height expressed in terms of the work functions of the two electrode materials, i.e., $\phi_{\text{eff}} \sim (\phi_{\text{Pt/Ir}}+\phi_{\text{HOPG}})/2$]. From Eq. (3), the change in tip-to-sample separation Δs at two different voltages can be estimated if κ_0 is known. Since the value of the barrier height varies with the tip-to-sample separation and may also be affected by the presence of contaminants, it is not possible to determine an absolute value for ϕ_{eff}; however, if ϕ_{eff} is assumed to remain constant in the bias voltage ranges used (0.24–0.10 V), then the absolute change in s can be calculated. For example, assuming $\phi_{\text{eff}} \sim 4$ eV and a constant tunneling current of 2.4 nA, reducing the voltage from 0.24 to 0.1 V corresponding to an $\sim$0.5-Å decrease in the tip-to- sample separation. A larger value in Δs would be expected if ϕ_{eff} were reduced by the presence of a contamination layer.[22] We speculate that this bias-dependent variation in tip-to-substrate distance influences the magnitude of the shear stresses acting on the surface while imaging.

The shear force necessary for dislocation movement can be calculated from the stacking-fault energy γ_{SFE}. Numerical values of γ_{SFE} can be obtained from the separation distance between pairs of parallel partial dislocations, such as those shown in the ribbon network in Fig. 2(c). Figure 7 shows an enlarged view of three sets of parallel ribbons, each ribbon being formed from a pair of partial dislocations whose separation ranges from 12 to 25 nm. The stacking-fault energy γ_{SFE} can be calculated from Eq. (4) (Ref. 23)

$$\gamma_{\text{SFE}}=[(2-3\nu_{\text{eff}})/(1-\nu_{\text{eff}})]\mu_{\text{eff}} b^2/8\pi d , \tag{4}$$

where d is the observed spacing between the partial dislocations and b is the modulus of the Shockley partial Burgers vector (0.142 nm). In conjugation with anisotropic elasticity theory (Appendix A), the elastic constants for graphite are as follows: Poissons ratio, $\nu_{\text{eff}}=0.34$ and the shear modulus, $\mu_{\text{eff}}=45.5\times10^9$ N/m^2. Using these values and the range of measured separation distances ($d=12$–25 nm), γ_{SFE} is estimated to be between 2.1 and 4.5 mJ/m^2. Analysis of previously published STM images[5] of a similar ribbon network yields $\gamma_{\text{SFE}}=1.5$–4.7 mJ/m^2.

The average value of γ_{SFE} obtained from our STM images is slightly larger than values obtained from

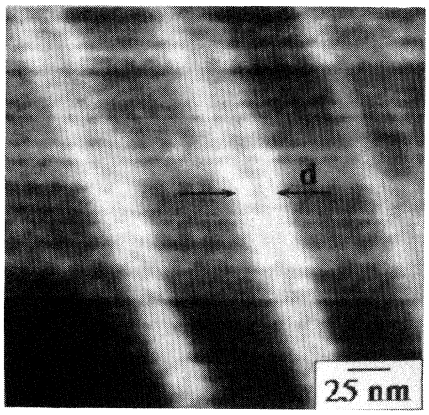

FIG. 7. A 250 ×250 nm STM image showing pairs of partial dislocations enclosing a ribbon of rhombohedral (faulted) graphite. The intrapair separation distance is marked by the arrows.

electron-microscopy images[24] (1.5 mJ/m^2; see Ref. 25). In contrast to electron-microscopy experiments where the observed partial dislocations may be tens to hundreds of angstroms below the surface, only dislocations at or within the first few layers of the surface are imaged in STM. According to Read[26] and others,[27,28] the width of the dislocation ribbons should decrease as they approach the surface due to the reduced elastic repulsion between the dislocations. Thus the energies of the surface stacking faults calculated from STM observations may be appreciably larger than the bulk values obtained by electron microscopy. However, it has been theorized that the stacking-fault energy should not change appreciably for very anisotropic materials, such as graphite, unless the fault is located very close to the surface.[30] Correcting for the surface proximity effect (Appendix B), we obtained $\gamma_{\text{SFE}}=0.14$–2.6 mJ/m^2 from our STM images, in good agreement with electron-microscopy results.

To estimate the force required for dislocation motion we consider the forces acting on the partial dislocations enclosing the stacking-fault ribbons. An elastic repulsion force between the partial dislocations F_{el} tends to separate the partial dislocations while an opposite stacking-fault force $F\gamma_{\text{SF}}$ tends to draw the partial dislocations together. The stacking-fault energy γ_{SFE} has units of energy per unit area (Nm/m^2), but can also be thought of as a force per unit length of a dislocation (N/m) which draws the partial dislocations together. The elastic repulsion force also equals the shear force per unit length τb multiplied by the length of the dislocation which is affected by the force L_{eff}. From Kelly and Groves,[29] the stacking-fault force is also equal to $\gamma_{\text{SFE}}d$, giving

$$F\gamma_{\text{SF}}(N)=F_{\text{el}}(N)=\tau b L_{\text{eff}}(N)=\gamma_{\text{SFE}} d(N) . \tag{5}$$

The field around the STM tip can be thought of as a repulsive force which destabilizes the partial dislocations from their equilibrium separation. Thus the tip acting on

a length of a dislocation L_{eff} causing it to move would exert an average shear stress of

$$\tau=\gamma_{\text{SFE}}d/bL_{\text{eff}} . \quad (6)$$

As a zero-order estimate of τ, we assume that L_{eff} is equivalent to the length of the base of the triangle between two bright points (75 nm), yielding $\tau=5$ MPa. (For comparison, macroscopic indentation experiments indicate that forces on the order of ~ 1 GPa damage the surface of graphite.[30]) Mate *et al.* have shown that forces between the tip and substrate on the order of 10^{-6}–10^{-7} N (~ 50–100 MPa for their assumed 80-nm tip contact radius) were required to obtain STM images.[31] In addition, Gilman[32] has estimated that dislocation motion can be achieved at room temperature if $\tau>\mu/100$ or 500 MPa. From this analysis, the shear force provided by the STM tip is both less than the force Mate *et al.* found necessary for tunneling and less than the force required for dislocation motion. The calculated value for τ using Eq. (6) can also be compared to the macroscopic average critically resolved shear stress for the basal plane of annealed HOPG which is ~ 0.6 MPa,[33] or approximately ten times less than the forces estimated from our STM experiment. At best, the calculation in Eq (6) is only a crude estimate as the tip is acting on a small portion of the dislocation line (which may be less than 75 nm) at one time. The value of 5 MPa could be considered a lower bound for τ. To estimate an upper bound for τ, one can take $L_{\text{eff}}=2$ nm (which assumes that only the section of the dislocation directly under the tip is moving), and obtain a value for τ of ~ 200 MPa, comparable to or larger than the above-mentioned estimates of the force necessary for dislocation motion and STM imaging. We conclude that the shear forces resulting from the tip are sufficient to cause the observed transitions between triangle- and star-shaped networks.

IV. SUMMARY

We have reported STM observations of a reversible, tip-induced transition between two different network geometries of partial dislocations on the basal plane of HOPG. The shear stress required for dislocation motion is comparable to previous estimates of the shear stress in STM experiments. Atomically resolved images near a dislocation show distortions in the lattice which are attributed to glide of the dislocation on the basal plane. In addition, dislocation motion was observed on the time scale of the STM experiment, allowing an estimate of the dislocation velocity. The capability of STM to image and control dislocation motion in real time may provide a new approach to probe, at the nanometer scale, the effects of various treatments (e.g., quenching and annealing) on the material's properties. For instance, it should be possible to observe how dislocation pinning by impurities or the interaction of dislocations with surface adsorbates affects dislocation motion and thus the elastic and plastic properties of the material.

ACKNOWLEDGMENTS

This work was supported by the Office of Naval Research, the Department of Energy, Basic Sciences Division (Grant No. DE-FG02-84ER45141) and by the Center for Interfacial Engineering with funding from the NSF Engineering Research Centers Program.

APPENDIX A: CALCULATION OF γ_{SFE}

The width d ($=12$–25 nm from Fig. 7) of a ribbon lying in the basal plane of an anisotropic hexagonal crystal is given by[26]

$$d=d_0\{1-[2\nu_{\text{eff}}/(2-\nu_{\text{eff}})]\cos 2\varphi\} \quad (A1)$$

with

$$d_0=[(2-\nu_{\text{eff}})/(1-\nu_{\text{eff}})]\mu_{\text{eff}}b^2/8\pi\gamma_{\text{SFE}} , \quad (A2)$$

where ν_{eff} is Poisson's ratio, φ is the angle between the total Burgers vector and the direction of the ribbon, d_0 is the equilibrium spacing between the partials, b is the modulus of the Shockley partial Burgers vector (0.142 nm), and μ_{eff} is the shear modulus. For a pure screw dislocation, φ is zero since the Burgers vector is parallel to the direction of the ribbon and so $d=d_0[1-(2\nu_{\text{eff}})/(2-\nu_{\text{eff}})]$. In an anisotropic medium, μ_{eff} and ν_{eff} must be calculated according to[26]

$$\mu_{\text{eff}}=[c_{44}/2(c_{11}-c_{12})]^{1/2} \quad (A3)$$

and

$$\mu_{\text{eff}}/(1-\nu_{\text{eff}})=(c_{11}c_{33}-c_{13}^2)/c_{33}(2\delta_1+\delta_2)^{1/2} , \quad (A4)$$

where

$$\delta_1=(c_{11}/c_{33})^{1/2} \quad (A5)$$

and

$$\delta_2=(c_{11}c_{33}-c_{13}^2-2c_{13}c_{44})/c_{33}c_{44} . \quad (A6)$$

In Eqs. (A3)–(A6), c_{ik} are the elastic constants for a system with the x_3 axis along the hexagonal axis. Values for c_{ik}, which are taken from Kelly[34] and listed below, are given as $c_{ik}=c_{ik}/10^{11}$ dyn cm^{-2}:

$$c_{11}=106,\quad c_{12}=18,\quad c_{13}=1.5 ,$$

$$c_{33}=3.65,\quad c_{44}=0.45 .$$

The Cauchy relations for central forces, i.e., $c_{13}=C_{44}$ and $c_{12}=1/2(c_{11}-c_{12})$, are not obeyed. The value for c_{44} shown above is for a perfect crystal with the glissile basal dislocations pinned out. The effects of twist boundaries, cross-links between adjacent layer planes, and specific dislocation configurations on the value of c_{44} are not known.

Using the above equations (A1)–(A6) in conjunction with the values for c_{ik}, $\mu_{\text{eff}}=45.5\times 10^{-9}$ N/m^2, $\nu_{\text{eff}}=0.34$, and $\gamma_{\text{SFE}}=2.1$–4.5 mJ/m^2.

APPENDIX B: CORRECTION OF γ_{SFE} FOR SURFACE PROXIMITY EFFECTS

Calculation of γ_{SFE} is based on the separation distance d between the partial dislocations in a ribbon. Siems, Delavignette, and Amelinckx[27] and Spence[28] have noted that d decreases as the ribbon approaches the surface due to the reduced elastic repulsion between the partials comprising the ribbon. They have obtained an analytical expression for the stress field of a screw dislocation parallel to a free surface which takes into account both the surface effects and anisotropy. The stacking-fault energy γ_{SFE} can be corrected for surface proximity effects[30] using the factor $[1-f]$, given by Eqs. (B1)–(B3),

$$\gamma_{SFE}(x \rightarrow \infty)=\gamma_{SFE}(z)[1-f] , \tag{B1}$$

where

$$[1-f]=[1-(1+4z^2\delta_3/x^2)^{-1}] \tag{B2}$$

and

$$\delta_3=(c_{11}-c_{12})/2c_{44} . \tag{B3}$$

The stress field at a distance from the partial dislocation, denoted by x, is taken as the observed separation between the pair of partial dislocations d ($=12-25$ nm in Fig. 7). z is the distance of the dislocation from the free surface and δ_3 takes into account the anisotropy of the material. In order to correct γ_{SFE} in the STM experiment for surface effects, we take z as equal to either one or two lattice interplanar c-axis spacings (0.335 or 0.67 nm, respectively). These values were chosen since the STM images reflect the structure of the first few layers of graphite. Using Eqs. (B1)–(B3) and the numerical result from Appendix A, we obtain $\gamma_{SFE}=0.14-2.6$ mJ/m^2 .

It is interesting to note that if one assumes that the value of γ_{SFE} obtained from electron-microscopy studies (1.5 mJ/m^2) is the correct value for the bulk stacking-fault energy (i.e., as $z \rightarrow \infty$), the separation distance between the partial dislocations found in the STM experiment (12–25 nm) corresponds to a depth from the surface z of 2.3–7.5 Å. This is consistent with our assumption that the stacking-fault network is located within the first few layers of the surface.

[1] C. Liu, H. Chang, and A. J. Bard, Langmuir **7**, 1138 (1991).
[2] H. Chang and A. J. Bard, Langmuir **7**, 1143 (1991).
[3] C. R. Clemmer and T. B. Beebe, Jr., Science **251**, 640 (1991).
[4] H. Lipson and A. R. Stokes, Proc. R. Soc. London Ser. A **181**, 101 (1942).
[5] S. R. Snyder, T. Foecke, H. S. White, and W. W. Gerberich, J. Mater. Res. **7**, 341 (1992).
[6] G. Bacon, Acta Crystallogr. **3**, 320 (1958).
[7] H. Jagodzinski, Acta Crystallogr. **2**, 298 (1949).
[8] P. Delavignette and S. J. Amelinckx, Nucl. Mater. **5**, 17 (1962).
[9] G. K. Williamson, Proc. R. Soc. London Ser. A **257**, 457 (1960).
[10] J. Garbarz, E. Lacaze, G. Faivre, S. Gauthier, and M. Schott, Philos. Mag. A **65**, 853 (1992).
[11] M. Kuwabara, D. R. Clarke, and D. A. Smith, Appl. Phys. Lett. **56**, 2396 (1990).
[12] Periodicities are measured by measuring the peak frequencies in line profiles drawn along the rows of bright spots.
[13] J. M. Soler, A. M. Baro, N. Garcia, and H. Rohrer, Phys. Rev. Lett. **57**, 444 (1986).
[14] H. J. Mamin, E. Ganz, D. W. Abraham, R. E. Thompson, and J. Clarke, Phys. Rev. B **34**, 9015 (1986).
[15] D. Tomanek and S. G. Louie, Phys. Rev. B **37**, 8327 (1988).
[16] P. Goodman, Acta Crystallogr. A **32**, 793 (1976).
[17] B. T. Kelly, *Physics of Graphite* (Applied Science, London, 1981), Chap. 2.
[18] J. Hirth and J. Lothe, *Theory of Dislocations,* 2nd ed. (Krieger, Malaar, FL, 1992), Chap. 19.
[19] D. Hull and D. J. Bacon, *Introduction to Dislocations,* 3rd ed. (Pergamon, New York, 1984), Chap. 3.
[20] E. J. Freise and A. J. Kelly, Philos. Mag. **8**, 1519 (1963).
[21] E. O. Kane, in *Tunneling Phenomena in Solids,* edited by E. Burnstein and S. Lundqvist (Plenum, New York, 1969), Chap. 1.
[22] J. H. Coombs and J. B. Pethica, IBM J. Res. Dev. **30**, 455 (1986).
[23] *The Direct Observation of Dislocations Solid State Physics Supplement 6,* edited by S. Amelinckx (Academic, New York, 1964), Chap. 10.
[24] R. Siems, P. Delavignette, and S. Alemlinckx, Z. Phys. **165**, 502 (1961).
[25] The stacking-fault energy γ_{SFE} in Ref. 27 is reported to be 0.7 mJ/m^2 based on the elastic constants given in C. Baker, Y. T. Chou, and A. Kelly, Philos. Mag. **6**, 1305 (1961). Using more recent estimates of elastic constants (Ref. 37) the data in Ref. 27 yield $\gamma_{SFE}=1.5$ mJ/m^2.
[26] W. T. Read, *Dislocations in Crystals* (McGraw-Hill, New York, 1953), Chap. 5.
[27] R. Siems, P. Delavignette, and S. Amelinckx, Phys. Status Solidi **2**, 636 (1962).
[28] G. B. Spence, J. Appl. Phys. **33**, 729 (1962).
[29] A. Kelly and G. W. Groves, *Crystallography and Crystal Defects* (Addison-Wesley, Reading, MA, 1970), Chap. 8.
[30] J. Skinner, N. Gane, and D. Tabor, Nature. Phys. Sci. **232**, 195 (1971).
[31] C. M. Mate, R. Erlandsson, G. M. McClelland, and S. Chiang, Surf. Sci. **208**, 473 (1989).
[32] J. J. Gilman, *Micromechanics of Flow in Solids* (McGraw-Hill, New York, 1969), Chap. 5.
[33] D. E. Soule and C. W. Nezbeda, J. Appl. Phys. **39**, 5122 (1968).
[34] B. T. Kelly, High Temp.-High Pressures **13**, 245 (1981).

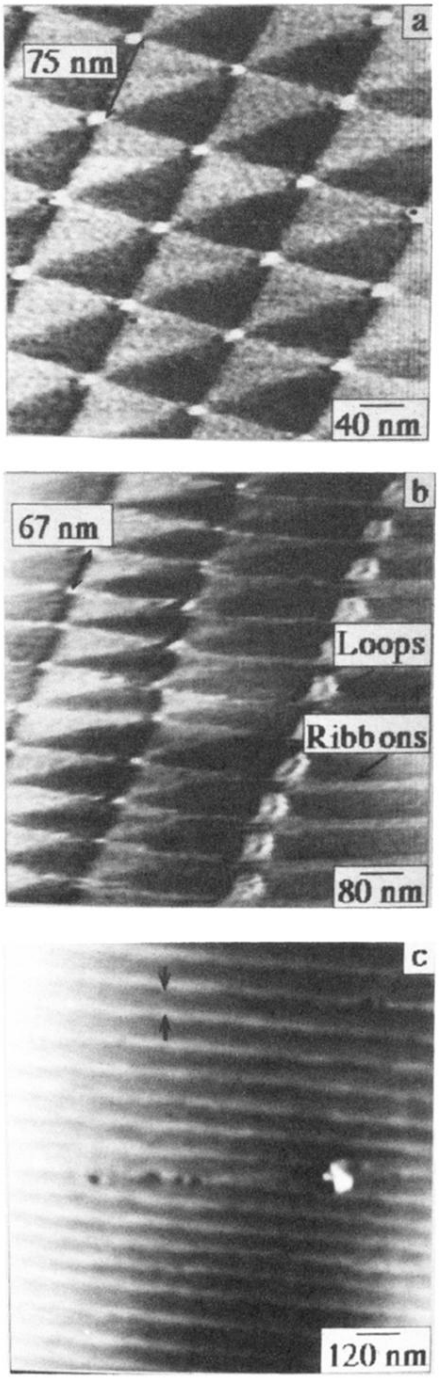

FIG. 2. STM image of (a) a 400 nm×400 nm area of a triangular array on the (0001) plane of HOPG. The array consists of alternating faulted (rhombohedral graphite, light triangular regions) and unfaulted (hexagonal, dark triangles). Sample bias voltage, tunneling current, and scan rate were 0.24 V, 0.37 nA, and 26 Hz, respectively. (b) 800 nm×800 nm area to the right of the array in (a) showing a row of prismatic dislocation loops which form the boundary between the triangular array and rows of ribbons. Sample bias voltage, tunneling current, and scan rate were 0.12 V, 0.6 nA, and 26 Hz, respectively. (c) 1200 nm×1200 nm area to the right of the triangular array showing a large area covered by rows of ribbons. The ribbons terminate at a defect site on the graphite. Sample bias voltage, tunneling current, and scan rate were 0.10 V, 0.78 nA, and 26 Hz, respectively.

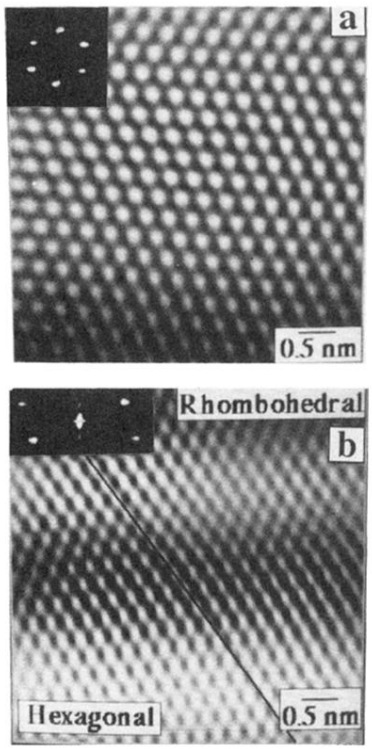

FIG. 3. (a) STM image of a 5 nm×5 nm area of a dark triangular region (unfaulted) showing the hexagonal arrangement of the graphite lattice. Bias voltage is 0.12 V and tunneling current is 0.7 nA. Inset: fast Fourier transform (FFT) of the image showing six bright spots characteristic of hexagonal graphite. Periodicities are 2.6 Å. (b) STM image of a 5 nm×5 nm area near the boundary between the lighter and darker triangular regions. The image shows glide of the basal plane by ~1 unit cell. Bias voltage is 0.25 V and tunneling current is 1.7 nA. Inset: FFT of the image in (b) showing four bright spots in a rectangular pattern. Periodicities are 2.4 and 2.8 Å.

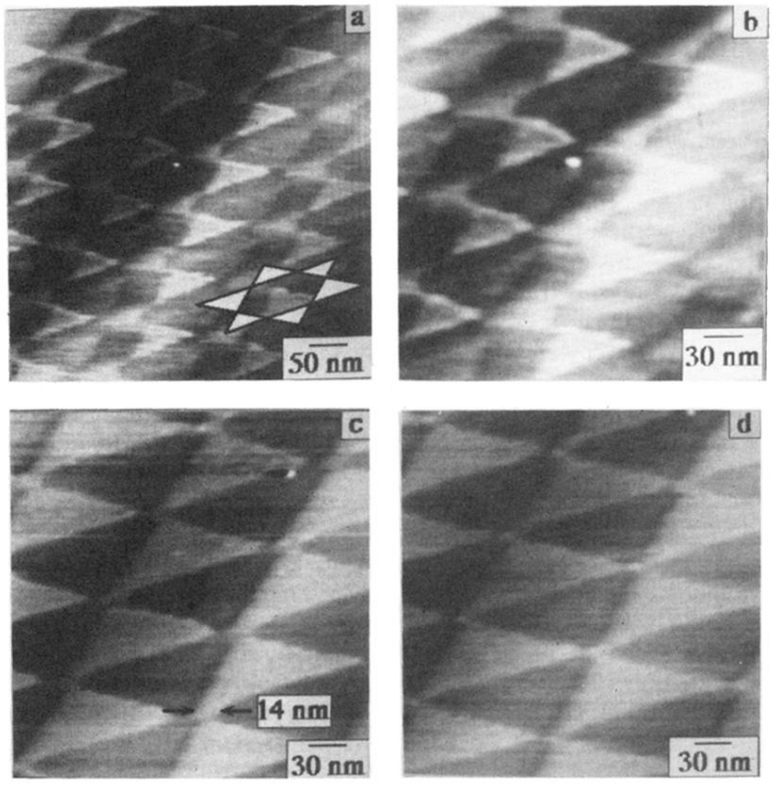

FIG. 4. STM images showing the voltage-induced transition of the star network to a triangular network as the bias voltage is changed from 0.10 to 0.24 V. [The white dot in the center of (a) can be used to identify the coordinates of the triangles in the sequence of images.] (a) 500×500 nm image of the star network obtained at 0.10 V. The star network is comprised of alternating small and large triangles pointing at 180° from one another. (b) 300 nm×300 nm image of the same area in (a). (c) 300 nm×300 nm image of the same area as in (b) showing the reappearance of the triangular network ~1 min after changing the bias voltage from 0.10 to 0.24 V. The triangles are no longer joined together at their vertices and the base of the triangles are trapezoidal shaped. (d) 300 nm×300 nm image of the same region taken 1 min later. The vertices of the triangles have intersected to form bright points. Tunneling currents are 2.4 nA and scan rates are 26 Hz.

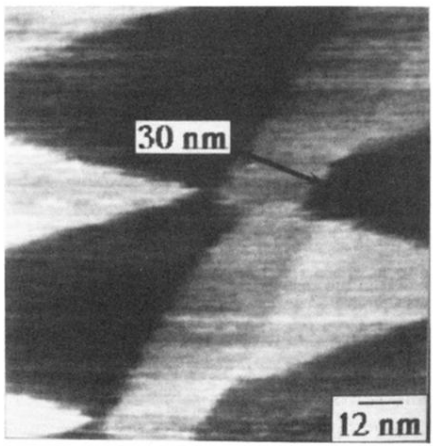

FIG. 5. A 125 nm $\times$ 125 nm STM image of the base region of a triangle showing the trapezoidal area of light contrast. Bias voltage is 0.24 V, tunneling current is 2.4 nA, and scan rate is 26 Hz.

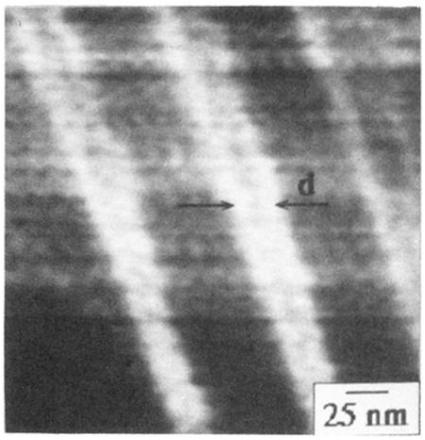

FIG. 7. A 250 ×250 nm STM image showing pairs of partial dislocations enclosing a ribbon of rhombohedral (faulted) graphite. The intrapair separation distance is marked by the arrows.